International Journal of Engineering and Applied Sciences (IJEAS)
Vol.2, Issue 4(2010)83-92

NUMERICAL STUDY OF FLOW STABILIZATION MECHANISM OF STEPPED-NOSED OBSTACLE

K. M. Rahman and M. Mashud
Department of Mechanical Engineering
Khulna University of Engineering & Technology (KUET)
Khulna-9203, Bangladesh, E-mail: russel_meek@yahoo.com

Received Date: 06 May 2010; Accepted Date: 23 July 2010

Abstract

A rectangular obstacle the front corners of which are deformed in step form (called "stepped nosed obstacle") may experience a much smaller drag force and lift force fluctuation. The underlying physics of this drag reduction and flow stabilization mechanism are explored in numerical and theoretical approaches. In the optimal step configuration that the flow separating from the front surface edges reattaches smoothly at the leading edge of the main body's side surface. (1) The pressure drag force acting on the forebody almost vanishes because the strong vortices trapped in the stepped corners produce the thrust force which cancel the drag force acting on the front surface, and (2) The oscillation of lift force acting on the obstacle is largely suppressed and the scale of the Karman vortices is reduced because the large scale of the separated flow over the side surface is suppressed. The step size which brings about such optimal step flow condition is identified and the dependences of various flow characteristics on the step size are discussed in detail, which will be useful to consider another drag reduction treatment than streamlining the profile of obstacle in engineering application.

Key Words: Drag Reduction, Numerical Simulation, Rectangular body, and Stepped nosed

1. Introduction

Drag force acts on an obstacle placed in a uniform stream. It consists of pressure drag, skin friction drag, and others. For blunt obstacle placed in an unbounded, high speed but low-mach number flow, the contribution of pressure drag due to fluid displacement by the obstacle is the most significant, and its magnitude strongly depends on the shape of the obstacle. The dynamic pressure of uniform flow is a good scaling factor of this drag force. The drag coefficient times the characteristics cross-sectional area of the obstacle may be regarded as an effective collision cross sectional area of the obstacle viewed from the uniform stream attacking the obstacle. Thus, a streamlined profile of the obstacle appears almost "transparent" to the uniform stream. In engineering application, there are, however, a lot of cases when blunt bodies are preferred from economical requirement and other reasons. Therefore, in this paper, we consider a method to reduce the pressure drag of blunt obstacle (typically, a rectangular obstacle placed parallel to a uniform stream, in two dimensional configuration) by changing its nose shape locally while preserving the overall shape of the obstacle. The most familiar method is that the sharp edges of

an angular nose are rounded out to obtain continuous variation in shape, which avoids the flow separation at the front corners. Interestingly, it is also possible to attain the same or more effective drag reduction by notching the front corner in step form because the local flow separation in the step regions may make a similar effect to the rounding-out of the sharp edges. Considering the cost of manufacturing curved surfaces and the resulting reduction of payload space, the hydrodynamics involved in this drag reduction method is especially worthwhile to examine in detail for engineering application.

It is well known that any obstacle placed in a uniform stream experiences no drag force if the surrounding inviscid flow does not separate from the obstacle. This paradox (d'Alembert paradox) emerges because the pressure forces acting on the front and back surface cancel out. It is interesting to note that the direction of these forces change depending on the geometry of the obstacle. For example, consider the two dimensional potential flow past a circular cylinder, in which a finite drag force acts on the upstream half and the same magnitude of thrust force, on the down stream half. On the other hand, a plate placed perpendicular to a uniform stream has an infinitely large thrust force on the front surface and infinitely large drag force on the back surface, because the contribution of pressure rise at the central part of the plate. Similar things occur for round and angular nose bodies, too. These examples suggest that sharp edges may be utilized to produce large thrust force acting on the forebody and to reduce the total drag force acting on the obstacle. The purpose of the present paper is to demonstrate such possibility and to explore the underlying physics through the two-dimensional numerical calculation of flow passing a rectangular obstacle, which has a stepped at both corners of forebody surface. There are several experimental evidences, which demonstrate the feasibility of the above-mentioned drag reduction method. In connection with the drag reduction of a tractor-trailer rig by means of a shield on the roof of the tractor, Saunder [1] studied the overall drag on a prism of circular cross-section shielded by a disk placed coaxially upstream. Findings from Koenig and Roshko's [2] experimental investigation of the shielding effect of various disk placed coaxially upstream of an axisymmetric, flat-faced cylinder are famous. Remarkable decrease of the drag of such a system was observed for certain diameter and gap ratios. For such optimum shielding, the stream surface, which separates from the disk, reattaches smoothly onto the front edge of the cylinder. Variation on the axisymmetric disk-cylinder configuration included a hemispherical front body, rounding of the front edge of the cylinder and a change from circular to square cross-section. The drag of the forebody could be drastically reduced by simply rounding its edges or corners sufficiently. A corner radius equal to one–eight the body diameter is sufficient to reduce the drag of the forebody face to nearly zero, provided the Reynolds number is large enough that premature laminar separation does not occur.

Furthermore, there are also experimental studies to reduce drag of after bodies by controlled separating flows by Viswanath [3]. Kentfield [14] showed that a multistep at after-body that utilizes the concept of controlled the separated flows can offer significant drag reduction; he found 60% base drag reduction compared to an (unmodified) blunt base using a three-step model at low speeds. Stepped after-bodies remove in a number of toroidal vortices, and in a broad sense, they may be identified with "separation control by trapped vortices" discussed by Ringleb [5] with one major difference. For achieving drag reduction, the vortices generated a

the annular steps have to be weak in contrast to a strong vortex, which is a major feature of separation control using a standing or a trapped vortex; locked after bodies [6], which involve a stable vortex between the base and a circular disk mounted downstream, utilize stepped nosed concept.
These examples are closely related to each other through the common underlying physics, which unfortunately have not been fully explored. This is the motivation of our study.

2. Computational model

In the calculation, all quantities were made dimensionless. The length, velocity, and time were made dimensionless using the obstacle width H_* and uniform velocity U_*. In the following analysis, the same symbol without subscript* will be used to denote the corresponding dimensionless quantity. Computational model used in the present study is illustrated in Fig. 1. A rectangular obstacle of width H_* and length ($H_* + \ell_*$) is placed in a uniform stream confined between two parallel frictionless walls at a distance of 5 H_* apart from either side of the obstacle. Each corner of the rectangular nose is shaped in a step form of length ℓ_* and height h_*, here after the obstacle will be called "step nose obstacle". The Reynolds number, Re, based on the obstacle width H_* and uniform velocity U_*, is assumed to be 10,000. Therefore, the flow around the obstacle becomes laminar but unsteady. The velocity is uniform at the channel inlet, while a free outflow condition is imposed at the channel outlet. The front face of obstacle is located at a distance of 5 H_* downstream of the channel inlet. The distance between the back face of obstacle and the channel outlet is 10 H_*. This computational model give 10 % in solid blockage, However, such solid blockage alter the free-stream velocity but slightly affected the flow phenomena of flow around two dimensional obstacle as describe in rectangular experiment by N. Djalili & I.S. Gartshore. We trust that this computational configuration is appropriate enough to simulate the unbounded, uniform flow past the step nose obstacle. For comparison, we shall also consider a square and rectangular obstacles.

In the present study, the construction of a step nose obstacle obeys the following rule. Jointing a rectangle of width ($H_* - 2\bar{h}$) and length ℓ_* with the front face of a square of H_*, we compose a rectangular obstacle with step notches of length ℓ_* and height h_* at its front corners. Two series of step nose obstacles will be considered to characterize the step nose effects on various flow characteristics: (i) Varying the step length ℓ_* for a fixed $h_* = 0.16\ H_*$ and (ii) Varying the step height h_* for a fixed $\ell_* = 0.16\ H_*$. For practical application, smaller step height is preferable, if effective. The choice of the fixed step height $h_* = 0.16\ H_*$ in the series (i) is for the convenience of our numerical study.

The fractional step method (Harlow and Welch 1965) with time splitting (Chorin 1968) was used to solve the two-dimensional Navier-Stokes equations. The mesh system had non-uniform grid resolution. The grid becomes gradually finer close to the obstacle surface in order to resolve the boundary layer structure developed on the forebody surface in particular. The total number of mesh point was about 60,000. The time step was 0.01×10^{-3} to 0.05×10^{-3} and the time was non dimensionalized by the obstacle width H_* and free-stream velocity U_*., $t = t_* H_*^{-1} U_*^{-1}$. The pressure convergence criterion ranged from 1.0×10^{-6} to 0.01×10^{-6}.

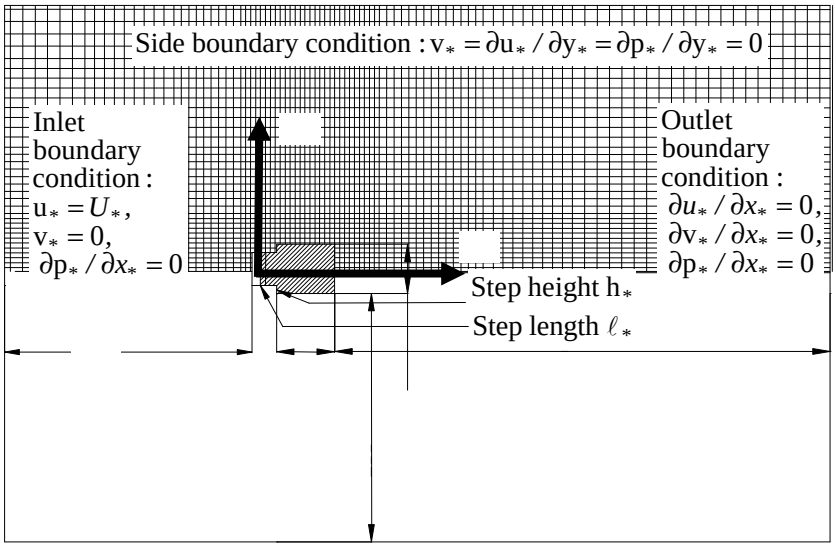

Fig.1. Computational Model

3. Numerical results and discussion

3.1 The effect of step height

Fixing the step length at □ =0.16, the step height h was varied from 0.0 to 0.5 to examine how the uniform stream impinging on the front face of the obstacle interacts with the step corners. The drag coefficient of the obstacle was calculated by integrating the time-average pressure coefficient over the all surfaces normal to the uniform stream. Figure 3(a) shows the step height dependence of the time-averaged drag coefficient and the contribution of each surface component. Since the length of obstacle is fixed in this series of calculations, the figure purely characterizes the step effects. The drag coefficient takes a minimum value at a step height nearly equal to 0.1. The net forebody drag, which is the sum of the contributions of front face and step walls, is almost zero at this step height. The net drag force is dominated by the drag force acting on the back surface. The drag coefficient of step nose obstacle (denoted as total in Fig. 3(a) is smaller than half the drag coefficient of the rectangular obstacle (at h = 0.0), which touches the step nose obstacle externally. It should be noted that this value is also less than the forebody drag coefficient 1.2 of two-dimensional round nose obstacle (Hoemer 1958). The figure indicates that the reduction of forebody drag causes the reduction of total drag. Thus, it is apparent that the drag reduction mechanism of the forebody changes the flow separation pattern (compare Fig. 2(a) and (b)) and reduces the drag force acting on the back surface. In the following, the underlying physics for this phenomenon will be explored in detail by viewing the pressure coefficient distribution plotted against distance measured along the obstacle surface starting from front surface and moving to the center of the back surface. Figure 4(a) shows the time-averaged pressure coefficient distribution around step nose obstacle for various step heights.

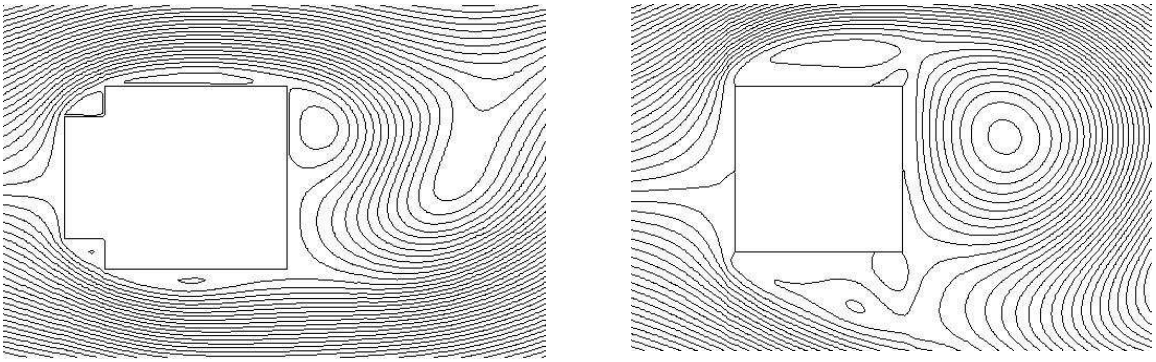

(a) (b)

Fig.2. (a) Step length and dead flow region pressure as functions of step height, (b) Thrust force acting on step walls as a function of step height.

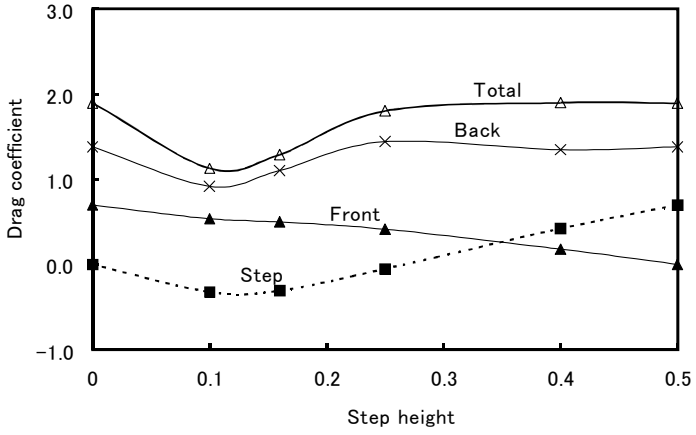

(a)

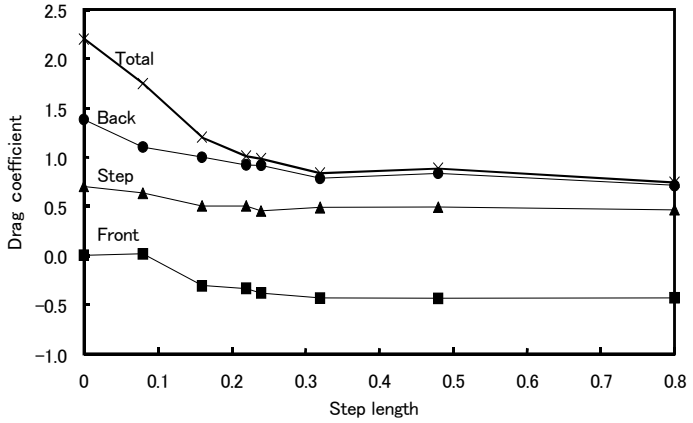

(b)

Fig.3. Pressure distribution along main body's sides

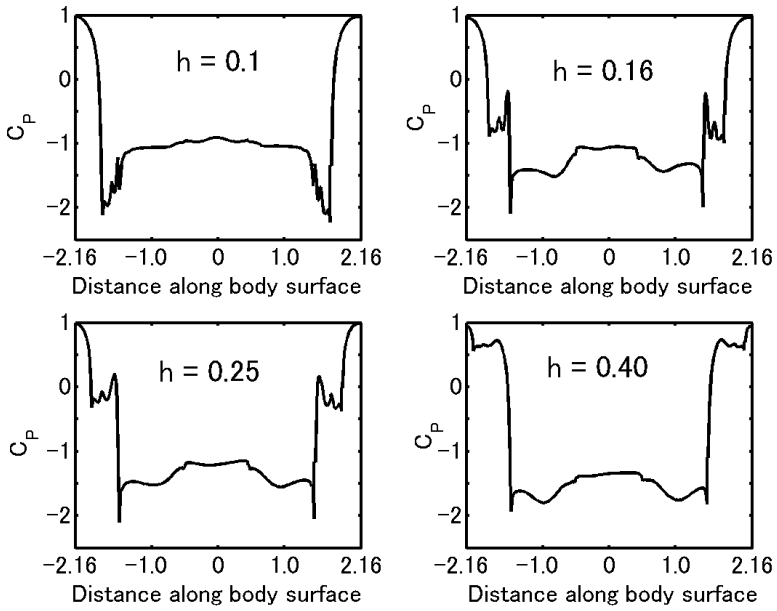

(a)

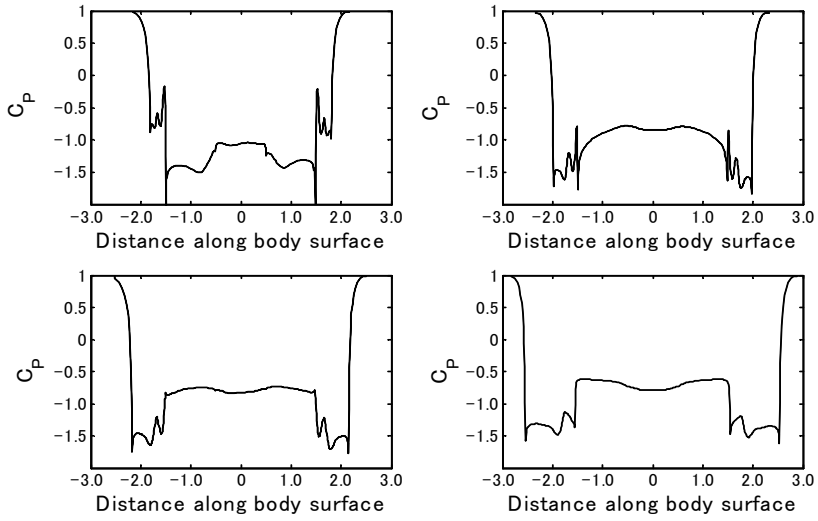

(b)

Fig.4. Velocity vectors and pressure contour (color) at an instant in quasi-steady state. (a) Square obstacle, (b) Step nose obstacle (h = 0.1 and ℓ = 0.16)

3.2. Lift Oscillation

Large lift coefficient fluctuations of a square obstacle are caused by the flow separation from the front corners, which is coupled with the wake flow oscillation. The suppression of this flow separation by the presence of step notches radically reduces the amplitude of lift coefficient fluctuation as seen in Fig. 5(b). The amplitude of fluctuation becomes minimum for the same condition as the time-averaged drag coefficient becomes minimum. Figure 5(b) shows the

dependence of lift coefficient fluctuation amplitude on step length. The amplitude becomes minimum at the step length which yields the minimum drag coefficient.

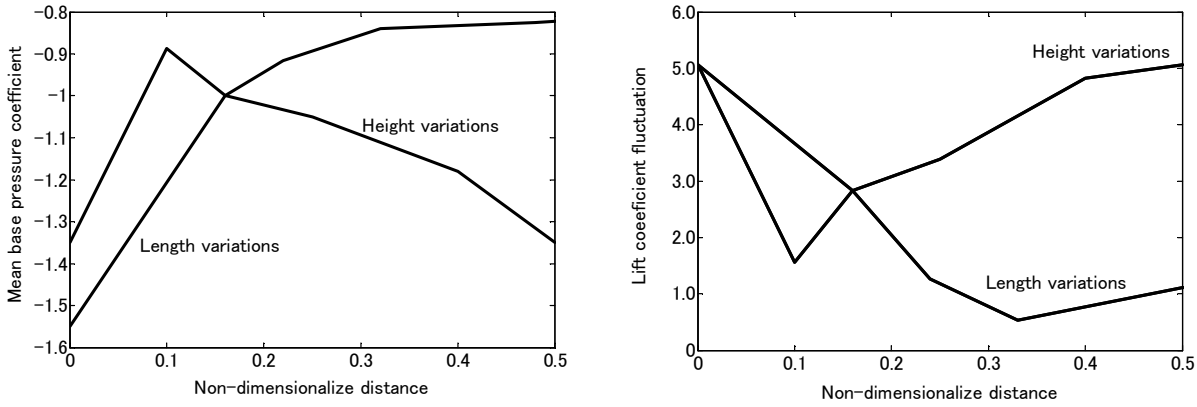

(a) (b)

Fig.5. Step heights Vs Lift Co-efficient

3.3 The effect of Step length

Fixing the step height at h = 0.16, the step length ℓ was varied to examine how the step corners interact with the separation bubbles which would be formed on both sides of the square obstacle in the absence of the step corners. In this series of calculations, the total length of step nose obstacle increases with step length. The variation of drag coefficient with step length includes the effect due to the enlargement of total length of step nose obstacle, which may be identified in comparison to the two rectangular obstacles touching the step nose obstacle internally and externally. Figure 3(b) shows the step length dependence of drag coefficient of step nose obstacle and contribution from each surface. In Fig 6, the drag coefficients of rectangular obstacles with length $1+\ell$ and widths 1 and 1-2h (Hoerner 1958) are drawn for comparison. As the step length increases from zero, the drag coefficient of step nose obstacle decreases and takes a minimum value at $\ell = 0.32$. A further increase in step length does not change the drag coefficient drastically. The drag coefficient of the front part slightly increases and then monotonically decreases with increasing step length in a similar way to the rectangular obstacles touching the step nose obstacle internally and externally, but it is considerably even smaller in comparison to the drag coefficient (non-dimensionalized by $0.5\rho_* U_*^2 H_*$) of the rectangular obstacle touching the step nose obstacle internally.

Figure 4(b) shows the pressure coefficient distribution along the stepped nosed obstacle surface with various step lengths. The velocity of the flow separating at the front corners is mainly determined by step height. However, the change in the step length alters the flow in the step region, and thus the pressure distribution on the side and back surfaces. The short step length case (ℓ=0.24) has a similar step flow structure to the large step height case discussed in the previous section. Part of the separated flow from the front corner impinges on the step wall and re-separates at the leading edge of side surface. The low-pressure part near the leading edge of side surface is due to this re-separated flow. Since, the re-separated flow velocity is not so

high; the separation bubble on the side surface has a small size. Downstream of it, the side surface pressure recovers to a certain value of back surface pressure in a similar way to the optimal step flow case (ℓ=0.32). On the other hand, in the cases of ℓ = 0.48 and 0.8, the flow which separates from the front corner reattaches at the leading edge of side surface at an angle, so that the pressure near the leading edge of side surface becomes nearly equal to, or slightly higher than, the back surface pressure (see Fig. 4(b)). Therefore, the side flow goes downstream without separation.

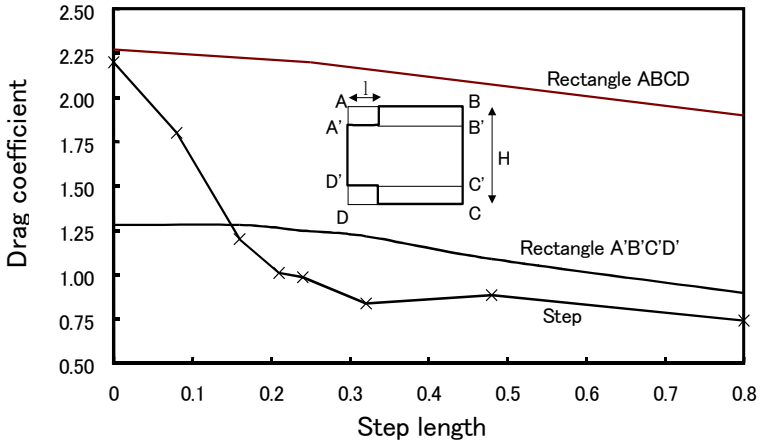

Fig.6. Step length dependence of time-averaged drag coefficient and contributions of surface parts relevant.

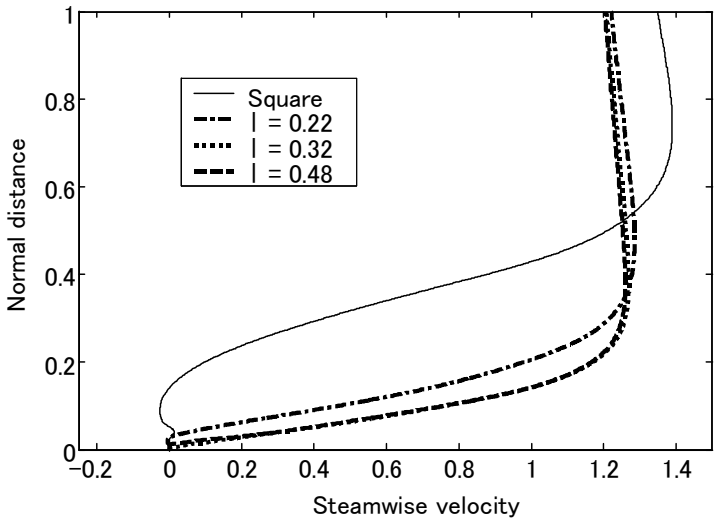

Fig.7. Comparison of drag coefficient of step nose obstacle to those of internally and externally touching rectangular obstacles

The degree of pressure variation along the side surface becomes small for larger step length. Thus, the same effect as the step nose obstacle with short side surface may be expected for a rectangular obstacle of width (1-2*h*) on which a pair of fins with height *h* are mounted at the same locations as the step walls of the step nose obstacle. In this case, the side surface of the

step nose obstacle is replaced by the free streamlines that are formed behind the fins. If these free streamlines are curved inward downstream, a further reduction in the drag force acting on the back surface will be attained. This is what is experimentally shown by Layukallo and Nakamura (2002), who found that a pair of fins with height 0.1, mounted at the distance 0.2 from the back surface, considerably reduced the drag coefficient of a rectangular obstacle placed in a transonic (Mach = 0.4) uniform stream

Figure 7 shows the axial velocity profile at the rear end of the side surface. The velocity increases from zero to a maximum value at a distance from the surface and then decreases to the uniform stream value. The laminar boundary layer that grows along the side surface ($\delta / H = 4.8 / \sqrt{Re} = 0.0048$) is much thinner than the distance between the side surface and the maximum velocity point. Therefore, the velocity profile illustrates the time-averaged feature of the unsteady separated flow. The flow separating from the front corners reattaches tangentially to the leading edges of side surface, the step region pressure is low. Therefore, there is an inverse pressure gradient along the side surfaces, and the flow may re-separate when the streamwise pressure gradient is too large. However, this flow separation is much smaller in scale, compared to the separated flow from the rectangular obstacle. It is important to note that all profiles of h > 0.32 collapse to a single curve, consistent with the invariance of back surface pressure with step length.

4. Conclusions

We have examined the flow around the step nose obstacles. The flow may be characterized by the separation property at each corner. The separating flow velocities, v_{max} and u_{max}, are the most important parameters to determine the flow characteristics of stepped nosed obstacle. The fluid impinging on the front surface turns its flow direction and flows along the front surface outward. In the optimal step flow condition when it reaches the step corners, the flow separates at the front face edge and reattaches at the leading edge of side surface of the main body. Then, a strong vortex is trapped in the step region, which produces suction pressure acting on the step wall. The thrust forces produced by this vortex as well as the flow acceleration due to the fluid exclusion by presence of the obstacle itself can cancel out some of the drag force acting on the front surface. As a result, the drag force of the stepped nosed obstacle becomes smaller than the drag of the rectangular obstacle of corresponding size. The net drag is dominated by the back surface pressure that increased by the effect of step corners. The optimal step avoids the large-scale flow separation from the body. Therefore, the amplitude of oscillation of lift coefficient is greatly suppressed. The following are worthwhile to note in particular:

The step not only reduces the drag force acting on the forebody but also suppress the large-scale flow separation from the obstacle. These effects due to pressure drop in the step region are caused by the flow acceleration due to the fluid displacement by the presence of body as well as the trap of strong vortices in the step regions. Because of viscous effects, the optimal step flow condition (when the flow separating from the front edge reattaches at the leading edge of the side surface) is realized for a rather wide range of step lengths when the step height is chosen appropriately.

References

[1] Kentfield, J.A.C, Short, Multi-step After Fairings, *J. Aircraft*, 12, 351-352, 1984.

[2] Koenig, K and Rosko, A., An experimental study of geometrical effects on the drag and flow field of two bluff bodies separated by a gap, *J. Fluid Mech*., 156, 167-204,1985.

[3] Morel, T., Theoretical lower limits of forebody drag, *Aero. J.*, 83, 23-27,1979.

[4] Ota, T., Asano, T. and Okawa, J., Reattachment length and transition of separated flow over blunt flat plates, *bulletin of the Japan Society for Mechanical Engineers*, 24, 941-947, 1981.

[5] Prandtl, L. and Tietjens, O.G., Applied Hydro-and Aeromechanics (translated by J.P. Hartog), SS77-81, Dover; 1934.

[6] Ringleb, F.O., Separation Control by trapped vortices, Boundary layer, and Flow control, *edited G.V. Lachmann, Pergamon*, Oxford, 265-294, 1961.

[7] Roshko, A., On the Wake and Drag of Bluff Bodies, *J. Aero. Sci.*. 22, 2-** , 1955.

[8] Saunders, W.D., Apparatus for reducing linier and lateral wind resistance in a tractor-trailer combination vehicle, U.S. Patent No. 3241876, 1966.

[9] Taylor, I. and Vezza, M., Prediction of unsteady flow around square and rectangular section cylinders using a discrete vortex method, *Journal of Wind Engineering and Industrial Aerodynamics*, 82 , 247 – 269, 1999

[10] Taylor, I. and Vezza, M., Calculation of the flow field around a square section cylinder undergoing forced transverse oscillations using a discrete vortex method, *Journal of Wind Engineering and Industrial Aerodynamics*, 82, 271 – 291, 1999

[11] Viswanath, P.R., Drag reduction of after bodies by controlled separated flows, *AIAA J.*, 39, 73-78, 2001.

[12] Watanabe, K., Characteristics of axial flow around step cylinder (parallel flow), *Trans. Japan Society of Mechanical Engineers*, B, 62, 2130-2136, 1996 (in Japanese).

[13] I. Taylor, M. Vezza, Calculation of the flow field around a square section cylinder undergoing forced transverse oscillations using a discrete vortex method. *Journal of Wind Engineering and Industrial Aerodynamics*, Vol. 82, P271 – 291, 1999